

Empirical estimation of host galaxy dispersion measure towards well localized fast radio bursts

Lucas Bernales-Cortes¹, Nicolas Tejos¹, J. Xavier Prochaska^{2,3,4,5}, Ilya S. Khrykin¹, Lachlan Marnoch^{6,7,8},
Stuart D. Ryder^{6,7}, and Ryan M. Shannon⁹

¹ Instituto de Física, Pontificia Universidad Católica de Valparaíso, Casilla 4059, Valparaíso, Chile
e-mail: lucas.bernales.c@mail.pucv.cl; nicolas.tejos@pucv.cl

² University of California, Santa Cruz, 1156 High St., Santa Cruz, CA 95064, USA

³ Kavli IPMU (WPI), UTIAS, The University of Tokyo, Kashiwa, Chiba 277-8583, Japan

⁴ Division of Science, National Astronomical Observatory of Japan, 2-21-1 Osawa, Mitaka, Tokyo 181-8588, Japan

⁵ Simons Pivot Fellow

⁶ School of Mathematical and Physical Sciences, Macquarie University, NSW 2109, Australia

⁷ Astrophysics and Space Technologies Research Centre, Macquarie University, Sydney, NSW 2109, Australia

⁸ Australia Telescope National Facility, CSIRO Space & Astronomy, Box 76 Epping, NSW 1710, Australia

⁹ Centre for Astrophysics and Supercomputing, Swinburne University of Technology, Hawthorn, VIC, 3122, Australia

January 27, 2025

ABSTRACT

Context. Fast radio bursts (FRBs) are very energetic pulses in the radio wavelengths that have an unknown physical origin. These can be used to study the intergalactic medium (IGM) thanks to their dispersion measure (DM). The DM has several contributions that can be measured (or estimated), including the contribution from the host galaxy itself, DM_{host} . This DM_{host} is generally difficult to measure, thus limiting the use of FRBs as cosmological probes and/or for understanding their physical origin(s).

Aims. In this work, we empirically estimate DM_{host} for a sample of twelve galaxy hosts of well-localized FRB at $0.11 < z < 0.53$, using a direct method based solely on the properties of the host galaxies themselves, referred to as $DM_{\text{host}}^{\text{direct}}$. We also explore possible correlations between DM_{host} and some key global properties of galaxies.

Methods. We use VLT/MUSE observations of the FRB hosts for estimating our empirical $DM_{\text{host}}^{\text{direct}}$. The method relies on estimating the DM contribution of both the FRB host galaxy's interstellar medium ($DM_{\text{host}}^{\text{ISM}}$) and its halo ($DM_{\text{host}}^{\text{halo}}$) separately. For comparison purposes, we also provide an alternative indirect method to estimate DM_{host} based on the Macquart relation ($DM_{\text{host}}^{\text{Macquart}}$).

Results. We find an average $\langle DM_{\text{host}} \rangle = 80 \pm 11 \text{ pc cm}^{-3}$ with a standard deviation of 38 pc cm^{-3} (in the rest-frame) based on our direct method, with a systematic uncertainty of $\sim 30\%$. This is larger than the typically used value of 50 pc cm^{-3} but consistent within uncertainties. We report positive correlations between DM_{host} and both the stellar masses and the star-formation rates of their hosts galaxies. In contrast, we do not find any strong correlation between DM_{host} and neither redshift nor the projected distances to the center of the FRB hosts. Finally, we do not find any strong correlation between $DM_{\text{host}}^{\text{direct}}$ and $DM_{\text{host}}^{\text{Macquart}}$, although the average values of the two are consistent within uncertainties.

Conclusions. Our reported correlations between $DM_{\text{host}}^{\text{direct}}$ and stellar masses and/or the SFRs of the galaxies could be used in future studies to improve the priors used in establishing DM_{host} for individual FRBs. Similarly, such correlations and the lack of a strong redshift evolution can be used to constrain models for the progenitor of FRBs, e.g. by comparing them with theoretical models. However, the lack of correlation $DM_{\text{host}}^{\text{direct}}$ and $DM_{\text{host}}^{\text{Macquart}}$ indicates that there may still be contributions to the DM of FRBs not included in our $DM_{\text{host}}^{\text{direct}}$ modeling, e.g. large DMs from the immediate environment of the FRB progenitor and/or intervening large-scale structures not accounted for in $DM_{\text{host}}^{\text{Macquart}}$.

1. Introduction

A fast radio burst (FRB) is a short (of the order of milliseconds), very energetic event ($\gtrsim 10^{39}$ erg) observed at radio wavelengths (Lorimer et al. 2007; Petroff et al. 2019; Cordes & Chatterjee 2019; Petroff et al. 2022). The progenitor and emission processes of FRBs remain unknown, although models implicating young magnetars (Michilli et al. 2018; Dall'Osso et al. 2024), or supernovae (Ouyed et al. 2020) have been favored over the last years (see Platts et al. (2019) for a compendium of theories). One of the key observational properties of FRBs is the dispersion measure (DM), which provides an estimate of the integrated column density of ionized matter along the line-of-sight to the pulse progenitor. The DM is defined as:

$$DM = \int \frac{n_e(l)}{1+z} dl, \quad (1)$$

where n_e is the density of free electrons, l is the line-of-sight path, and z is the redshift.

Having well-localized ($\lesssim 1''$) FRBs with identified host galaxies allows us to study and understand the observed DM_{FRB} of a given FRB in terms of the contributions from different cosmological scales (Macquart et al. 2020). We can expand DM_{FRB} as

$$DM_{\text{FRB}} = DM_{\text{MW}} + DM_{\text{cosmic}}(z) + \frac{DM_{\text{host}}^{\text{rest}}}{1+z}, \quad (2)$$

with

$$DM_{\text{MW}} \equiv DM_{\text{MW}}^{\text{ISM}} + DM_{\text{MW}}^{\text{halo}}, \quad (3)$$

where $DM_{\text{MW}}^{\text{ISM}}$ is the contribution from the Galactic interstellar medium (ISM), $DM_{\text{MW}}^{\text{halo}}$ is the contribution from the Milky Way halo, $DM_{\text{host}}^{\text{rest}}$ is the contribution from the host galaxy in its rest-frame including its halo, ISM and any gas local to the event itself, and $DM_{\text{cosmic}}(z)$ is the contribution from all other extragalactic gas, like the ionized gas in the large scale structure of the Universe and intervening halos of galaxies intersecting the FRB sightline (if any).

The ISM of the Milky Way is typically characterized using observations of the pulsar population, leading to the NE2001 (Cordes et al. 2003) and YMW16 (Yao et al. 2017) Galactic electron density models. The average DM_{cosmic} component, (DM_{cosmic}), follows the Macquart relation (Macquart et al. 2020), which relates the redshift of the FRB host galaxy with the $DM_{\text{cosmic}}(z)$.

For the $DM_{\text{host}}^{\text{rest}}$ contribution, it is common to use a fixed value (e.g. $DM_{\text{host,fix}}^{\text{rest}} = 50 \text{ pc cm}^{-3}$; Arcus et al. 2020, and references therein), or estimate it from a probability density function (PDF) expectation in the context of a Bayesian framework (typically log-normal, e.g. Macquart et al. 2020; James et al. 2022a; James et al. 2022b; Khrykin et al. 2024b). Alternatively, other authors (e.g. Marcote et al. 2020; Niu et al. 2022; Lee et al. 2023) estimate it by re-writing Equation 2 to solve for $DM_{\text{host}}^{\text{rest}}$ (see Section 3.2). However, a single $DM_{\text{host}}^{\text{rest}}$ value, or range (e.g. James et al. 2022b), for *all* FRB hosts (even at the same redshift) is not physically motivated because one expects local factors to directly affect the $DM_{\text{host}}^{\text{rest}}$ value such as local density, clumpiness, ionization state, etc.; similarly, the mass of the galaxy, the temperature of its halo, and the 3D position of the FRB source with respect to the observer must also affect the intrinsic DM_{host} value.

More direct estimations of DM_{host}^1 exist, which explicitly attempt to take into account the contribution of the galaxy host ISM via nebular emission lines. For instance Tendulkar et al. (2017) obtained an estimate of $55 \leq DM_{\text{host}}^{\text{obs}} \leq 225 \text{ pc cm}^{-3}$ at $z = 0.19$ based on $H\alpha$ for FRB20121102A. Similarly, Chittidi et al. (2020) obtained $DM_{\text{host}}^{\text{obs}} = 150 \pm 45 \text{ pc cm}^{-3}$ with the same method for the galaxy host of FRB20190608B at $z = 0.117$. Bannister et al. (2019) estimate $30 \leq DM_{\text{host}}^{\text{obs}} \leq 81 \text{ pc cm}^{-3}$ for the host galaxy of FRB20180924B at $z = 0.32$ using a Bayesian framework. In all these methods the uncertainty on DM_{host} is large, and its value is difficult to determine precisely. It is therefore important to investigate whether we can better (if at all) determine DM_{host} , which motivates our present study.

Our goal is to obtain an empirical estimate for this DM_{host} component, referred to as $DM_{\text{host}}^{\text{direct}}$, in a sample of several FRBs and analyzed in a homogeneous manner. In principle, in order to fully understand how the host galaxy affects DM_{host} , it is essential to consider not only the global properties of the galaxy but also the local environment of the FRB. Indeed, the specific region from which the FRB originates can significantly influence the interpretation of observational data and the understanding of the physical mechanisms involved (Mannings et al. 2021; Woodland et al. 2024). For addressing this, in this work we explore if there is any difference in using nebular gas emission from the

“global” ISM (full galaxy) or “local” to the source (at the position of the FRB). Furthermore, we also investigate some possible relations between this $DM_{\text{host}}^{\text{direct}}$ and internal properties of the host galaxies like stellar mass, star formation rate (SFR), as well as the geometry between the FRB and the host galaxy (e.g. projected distance of the FRB position and the galaxy center).

Our paper is structured as follows. In Section 2 we present the observational data utilized and the sample analyzed in this study, including some key properties of the host galaxies. In Section 3 we elaborate on our direct method as well as a previous (indirect) method to estimate the DM_{host} . In Section 4 we report the results and discuss them, while in Section 5 we provide the summary and main conclusions. In this work, we assume a flat Λ CDM cosmology with parameters consistent with the latest Planck 2018 measurements (Planck Collaboration et al. 2020).

2. Data

2.1. Sample

We use a sample of eleven well-localized FRBs detected by the Commensal Real-Time ASKAP Fast-Transients (CRAFT; Macquart et al. 2010) survey with identified host galaxies for which we have VLT/MUSE data (see below). We require better than 1'' of precision in the FRB localization, and to make a confident host galaxy association we require a Probabilistic Association of Transients to their Hosts (PATH; Aggarwal et al. 2021) posterior probability greater than 90%. In addition to ASKAP FRBs, we have also included FRB20210410D detected by the More TRAnsients and Pulsars (MeerTRAP; Rajwade et al. 2022) project which also satisfies the above criteria. Our final sample is composed of twelve FRB host galaxies and is summarized in Table 1.

2.2. Previous observations

The Fast and Fortunate for FRB Follow-up (F⁴) is a collaboration endeavoring to obtain dedicated photometric and spectroscopic follow-up observations of localized FRBs and their host galaxies. All the observational data of our studied host galaxies except $H\alpha$ fluxes (e.g. stellar masses, SFRs, FRB offsets), come from previous work done by F⁴ (see last column of Table 1 for specific references) and are available on both the FRB GitHub repository² (Prochaska et al. 2023) and the ‘FRB Hosts’ website³. We note that some values have been updated since their discovery papers, and here we used those reported by Gordon et al. (2023) and Shannon et al. (2024).

2.3. VLT/MUSE observations and data reduction

We wish to study the DM_{host} empirical contribution, and for this we use the Multi Unit Spectroscopic Explorer (MUSE; Bacon et al. 2010) mounted on UT4 (Yepun) at the Very Large Telescope (VLT) on Cerro Paranal, Chile. MUSE provides resolved or partially resolved integral-field spectroscopy which allows for a ‘local’ estimation of the ISM contribution to the host $DM_{\text{host}}^{\text{ISM}}$ based on the $H\alpha$ nebular emission at the FRB position (when available; see Section 3.1), and a ‘global’ estimation based on the $H\alpha$ nebular emission of the entire galaxy.

All the MUSE observations were conducted with the wide field mode (WFM) with adaptive optics and nominal wavelength

¹ In the following, we will refer to $DM_{\text{host}}^{\text{rest}}$ as DM_{host} unless otherwise noted. The relation between $DM_{\text{host}}^{\text{rest}}$ in the observer-frame versus in the source-frame is $DM_{\text{host}}^{\text{obs}} = DM_{\text{host}}^{\text{rest}}/(1+z)$.

² <https://github.com/FRBs/FRB>

³ <https://www.frb-hosts.org/>

FRB name	Redshift	DM _{total} (pc cm ⁻³)	RA FRB (deg)	Dec FRB (deg)	Host probability (%)	Reference
(1)	(2)	(3)	(4)	(5)	(6)	(7)
FRB20180924B	0.3212	362	326.1052	-40.9000	99.9	Bannister et al. (2019)
FRB20190102C	0.2912	365	322.4157	-79.4757	98.0	Bhandari et al. (2020)
FRB20190608B	0.1178	340	334.0199	-7.8982	99.9	Chittidi et al. (2020)
FRB20190611B	0.3778	333	320.7456	-79.3976	100.0	Day et al. (2020)
FRB20190711A	0.5217	595	329.4192	-80.3580	97.3	Heintz et al. (2020)
FRB20190714A	0.2365	504	183.9797	-13.0210	100.0	Heintz et al. (2020)
FRB20191001A	0.2340	507	323.3517	-54.7483	100.0	Heintz et al. (2020)
FRB20200430A	0.1610	380	229.7065	12.3763	100.0	Heintz et al. (2020)
FRB20200906A	0.3688	578	53.4955	-14.0830	100.0	Bhandari et al. (2022)
FRB20210117A	0.2145	730	339.9792	-16.1514	99.8	Bhandari et al. (2023)
FRB20210320C	0.2797	385	204.4587	-16.1227	100.0	James et al. (2022a)
FRB20210410D	0.1415	575	326.0862	-79.3182	99.6	Caleb et al. (2023)

Table 1. Sample of FRBs. (1) Name of the FRB; (2) Host redshift; (3) Total dispersion measure observed; (4) and (5) Right Ascension and Declination of the FRB (J2000), respectively; (6) PATH posterior probability of the putative host; (7) Discovery paper reference for each FRB; note that some values reported in this table have been updated according to Gordon et al. (2023) and Shannon et al. (2024).

range (AO-N) mode. This setup provides a field of view (FoV) of $1' \times 1'$ with a spatial sampling of $0.2'' \text{ pix}^{-1}$, and spectral coverage of $\approx 4700 - 9300 \text{ \AA}$, with resolving power ranging from $R \approx 1770$ at 4800 \AA to $R \approx 3590$ at 9300 \AA . We observe each field for $\sim 4 - 8 \times 600 \text{ s}$ individual exposures with typical DIMM seeing conditions of $\approx 1''$, which translated to $\lesssim 0.8''$ PSF thanks to the enabled AO. Table 2 summarizes the dates, exposure times and program IDs of the observations.

Data reduction was performed using the ESO MUSE pipeline (Weilbacher et al. 2020, v2.8.6.) within the ESO Recipe Execution Tool (EsoRex) environment (ESO CPL Development Team 2015). We used standard procedure and parameters.

3. Analysis

3.1. Direct DM_{host} estimation, DM_{host}^{direct}

Here we provide a direct estimate of DM_{host}^{direct}. For this estimation we consider two contributions, DM_{host}^{ISM} and DM_{host}^{halo}, giving

$$\text{DM}_{\text{host}}^{\text{direct}} = \text{DM}_{\text{host}}^{\text{ISM}} + \text{DM}_{\text{host}}^{\text{halo}}, \quad (4)$$

where DM_{host}^{ISM} includes gas from the ISM of the galaxy host plus any possible gas associated to the FRB progenitor itself, while DM_{host}^{halo} is the contribution from the galactic halo, both defined in the source frame. The methodology to estimate these two contributions is presented as follows.

3.1.1. Estimating DM_{host}^{ISM}

To estimate DM_{host}^{ISM} for the different galaxy hosts, we adopt the procedure outlined by Tendulkar et al. (2017) following Reynolds (1977). For completeness, we include the key equations here.

From the H α flux measured by MUSE, we obtain the H α surface brightness, $S(\text{H}\alpha)$, by dividing the H α line emission by the effective area considered.

We correct the emission for the Galactic dust extinction (Fitzpatrick & Massa 2007) and by surface brightness dimming in order to pass from the observer's frame to the source's

⁴ With a gap between $5760 - 6010 \text{ \AA}$ due to the contamination produced by the Sodium laser used for AO.

frame. From $S(\text{H}\alpha)$, in the source's frame, we use equation 10 of Reynolds (1977) to obtain an estimate of the emission measure (EM):

$$\text{EM}(\text{H}\alpha) = 2.75 \text{ pc cm}^{-6} T_4^{0.9} \left[\frac{S(\text{H}\alpha)}{\text{Rayleigh}} \right]. \quad (5)$$

Then, we adopt equation 5 from Tendulkar et al. (2017) to estimate DM_{host}^{ISM}, in the source's frame,

$$\text{DM}_{\text{host}}^{\text{ISM}} = 387 \text{ pc cm}^{-3} L_{\text{kpc}}^{1/2} \left[\frac{f_f}{\tau(1 + \zeta^2)/4} \right]^{1/2} \left(\frac{\text{EM}}{600 \text{ pc cm}^{-6}} \right)^{1/2}, \quad (6)$$

where f_f is the volume filling-factor of clouds, ζ represents the fractional density variation within any given cloud of ionized gas due to turbulence inside clouds, and τ is the density variation between any two clouds, all over a path length L_{kpc} in kpc (Cordes et al. 2016; Tendulkar et al. 2017; Chittidi et al. 2020).

Equation 6 has been calibrated in the Milky Way and may not necessarily apply to FRB hosts in general. More fundamentally, even within the Milky Way, the clumpiness and density variations can vary significantly between sightlines and thus this estimation is inherently uncertain. Therefore, the exact values of the parameters governing DM_{host}^{ISM} are unknown. In what follows we assume a turbulent and dense environment in the sightline, that is, the volume filling-factor is maximum ($f_f=1$) and that each ionized cloud along the sightline has internal density variations dominated by turbulence ($\zeta=1$) and that the variation between clouds is maximum ($\tau=2$). Finally, we assume that the FRB comes from a path width similar to the Milky Way disk, that is, $L_{\text{kpc}}=0.15$. In Section 4.5 we quantify the effect of these systematic uncertainties on our overall results.

3.1.2. Global and local DM_{host}^{ISM}

To provide a global estimation for DM_{host}^{ISM}, we use the H α nebular emission within the area defined by an ellipse with the reported eccentricity and by using the galaxy's effective radius as the semi-major axis, referred to as DM_{host}^{ISM,global}.

In addition, to have a more relevant DM_{host}^{ISM} estimation, we use the local nebular emission of H α coincident with the FRB

FRB name (1)	Obs. Dates (UT) (2)	Exp. time (s) (3)	Program ID (4)
FRB20180924B	2018 Nov 05 / 2019 Dec 06	8×600	2102.A-5005(A) / 104.A-0411(A)
FRB20190102C	2022 Oct 15	4×600	110.241Y.001
FRB20190608B	2022 July 29	8×600	105.20HG.001
FRB20190611B	2021 July 02	7×600	105.20HG.001
FRB20190711A	2021 July 02 / 2021 Ago 10	8×600	105.20HG.001
FRB20190714A	2021 Apr 18 / 2022 Feb 05	8×600	105.20HG.001
FRB20191001A	2022 Oct 1 / 2022 Oct 16	8×600	110.241Y.001
FRB20200430A	2023 Mar 31	8×600	110.241Y.002
FRB20200906A	2022 Nov 26 / 2022 Nov 29	8×600	110.241Y.002
FRB20210117A	2022 Oct 03	4×600	110.241Y.001
FRB20210320C	2023 May 11 / 2023 Jun 23	8×600	110.241Y.002
FRB20210410D	2022 Oct 22 / 2022 Oct 25	8×600	110.241Y.001

Table 2. Summary of MUSE observations. (1) Name of the FRB; (2) Date of the observations; (3) Exposure time; (4) Program ID(s).

position, referred to as $DM_{\text{host}}^{\text{ISM,local}}$. We obtain the local $H\alpha$ emission from the MUSE datacubes, by selecting a region of radius 0.4 arcsec (2 native spaxels) which corresponds to the typical seeing (comparable to or larger than the typical FRB positional uncertainty in our sample). Then, from this region we extract the spectrum at the observed wavelengths corresponding to the $H\alpha$ transition by summing the flux of all the spaxels with equal weight. We model the continuum by a spline which is subtracted from the observed spectrum. Then we model the remaining emission line flux with a Gaussian fit. Figure 1 shows an example for FRB20191001A. The FRB localization is denoted by the blue circle. In the lower panel of the figure we have the extracted 1D spectrum within the region, at the wavelengths corresponding to the observed $H\alpha$ emission, together with our modeled Gaussian fit and continuum. Finally we integrate the Gaussian fit to obtain the total $H\alpha$ nebular emission flux and its error.

Table 3 summarizes our results obtained for the global and local $DM_{\text{host}}^{\text{ISM}}$ estimates, and Figures A.1 to A.11 in the Appendix show the $H\alpha$ maps and emission lines for the rest of the sample.

Uncertainties in these estimations are calculated as follows: We do 10^5 realization of $H\alpha$, following a normal distribution around the given/calculated $H\alpha$ for every FRB host, with the error of $H\alpha$ as standard deviation; then, with every realization we repeat the previous steps to provide an empirical 1σ uncertainty from the resulting PDF.

For the host galaxy of FRB20190711A at $z = 0.522$, the MUSE spectrum does not cover the redshifted $H\alpha$ wavelength. In this case we follow a procedure similar to that used by Logroño-García et al. 2019, Calzetti et al. 2000 and Chittidi et al. 2020. We first obtained the $H\beta$ flux and $H\gamma$ analogously. We then estimate the extinction from the observed ratio of $H\gamma$ to $H\beta$ flux (0.397), and by comparing it to the theoretical value (0.466, Osterbrock & Ferland 2006). This gives us an extinction estimate of $A_v = 0.18$. Then with the extinction we can calculate the intrinsic ratio of $H\alpha$ to $H\beta$ flux following Calzetti et al. 2000; Logroño-García et al. 2019 to obtain a ratio of 4.364. Finally, this ratio gives us our estimate of $H\alpha$ (corrected for dust).

Given Equations 5 and 6, besides geometrical factors and temperature, the key observable for inferring $DM_{\text{host}}^{\text{ISM}}$ is the $S(H\alpha)$. In our case we obtain $S(H\alpha)$ for global (full galaxy) and local (at the FRB position) $H\alpha$, and a comparison between the two is shown in Figure 2. We observe that the global measurement is systematically larger than the local one. The dark-orange line shows the linear correlation between them, from which we infer a systematic difference of 19%, which translates to $\approx 14\%$ in the inferred $DM_{\text{host}}^{\text{ISM}}$ (see Equations 5 and 6).

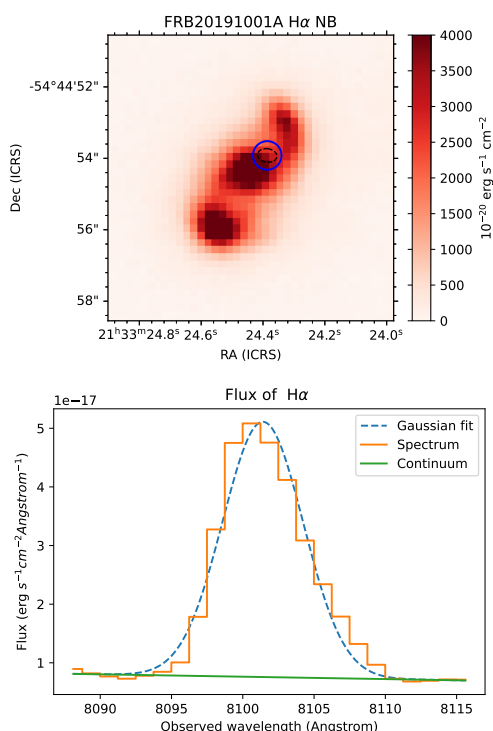


Fig. 1. Upper: FRB20191001A host emission integrated at the narrow band (NB) encompassing $H\alpha$ using the same wavelength range as shown in the bottom panel. The blue circle is centered at the FRB localization and has a radius of 0.4'' and the dashed black ellipse represents the actual FRB position uncertainty. Lower: The integrated spectrum of the $H\alpha$ emission within the blue circle (orange). We fit this emission with a Gaussian (dashed blue) plus a continuum (green).

3.1.3. $DM_{\text{host}}^{\text{halo}}$

For estimating $DM_{\text{host}}^{\text{halo}}$ we follow the procedure similar to Prochaska & Zheng 2019, Simha et al. 2023 and Chittidi et al. 2020. From the published estimated stellar mass for each host galaxy, we implement the abundance matching technique to infer a halo mass (Moster et al. 2013). Then, following Prochaska & Zheng (2019), we can estimate $DM_{\text{host}}^{\text{halo}}$ assuming a density profile for the halo gas. We used the modified Navarro, Frenk & White (mNFW) profile described by Prochaska & Zheng (2019) following Mathews & Prochaska (2017),

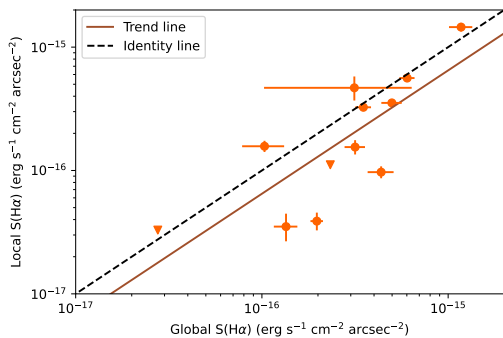


Fig. 2. Comparison between the local and global inferred surface brightness of H α , obtained from MUSE cubes, for our sample. The trend line (dark orange) has a slope of 1 by construction. The identity line (dashed line) corresponds to the 1:1 relation.

$$\rho_b = \frac{\rho_b^0}{y^{1-\alpha}(y_0 + y)^{2+\alpha}} \quad (7)$$

where $y_0 = 2$ and $\alpha = 2$, $y \equiv c(r/r_{200})$, with c being the concentration parameter and r_{200} is defined as the radius within which the average density is 200 times the critical density. Because we expect that not all of this gas is ionized, we need to estimate the fraction of baryons that are ionized (f_{hot}). For this, we use $f_{\text{hot}} = 55\%$ (Khrykin et al. 2024a) as a fiducial value to calculate ρ_b^0 , which corresponds to the density of the ionized mass.

With ρ_b , we can calculate the density of free electrons, n_e as:

$$n_e = \mu_e \frac{\rho_b}{m_p \mu_H} \quad (8)$$

with m_p the proton mass, $\mu_H = 1.3$ the reduced mass (accounting for Helium) and $\mu_e = 1.167$ accounts for fully ionized Helium and Hydrogen. Corrections for heavy elements are negligible.

This profile is integrated along the line-of-sight, from the projected distance R of the FRB, to the max radius of the halo (r_{200}). The $\text{DM}_{\text{halo}}(R)$ value is defined as:

$$\text{DM}_{\text{halo}}^{\text{halo}}(R) = \int_0^{\sqrt{r_{200}^2 - R^2}} n_e ds \quad (9)$$

where the lower integration limit corresponds to the mid-plane of the halo, which is perpendicular to the line of sight. Finally we evaluate Equation 9 to obtain $\text{DM}_{\text{halo}}^{\text{halo}}$ in the source's frame.

To account for uncertainties in $\text{DM}_{\text{halo}}^{\text{halo}}$ estimations derived from stellar mass for each host galaxy, we generate 1000 realizations of stellar masses, assuming a log-normal distribution where the standard deviation corresponds to the stellar mass uncertainty. For each stellar mass realization, we generate 100 additional realizations, varying the 8 parameters of the Moster relation. The mean values and standard deviations for these parameters are taken from table 1 of Moster et al. (2013), following a normal distribution. Finally, we obtain a PDF of $\text{DM}_{\text{halo}}^{\text{halo}}$ with 10^5 realizations per FRB, and use the 1σ of this PDF as our final uncertainty. As an example, Figure 3 shows this PDF for FRB20191001A.

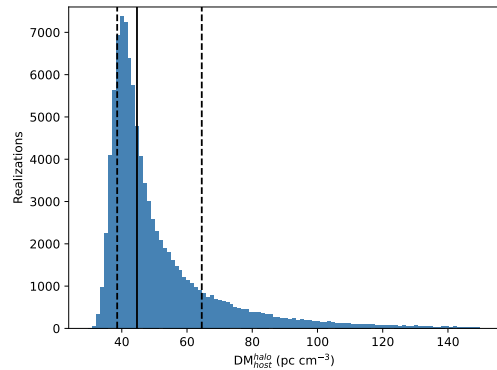


Fig. 3. Distribution of $\text{DM}_{\text{halo}}^{\text{halo}}$ for FRB20191001A. The vertical black solid line represents the median value and the dashed black lines the corresponding 16th and 84th percentiles.

3.1.4. Estimating $\text{DM}_{\text{host}}^{\text{direct}}$

To obtain $\text{DM}_{\text{host}}^{\text{direct}}$ we add the two PDFs of $\text{DM}_{\text{halo}}^{\text{halo}}$ and $\text{DM}_{\text{host}}^{\text{ISM}}$. From this sum, we generate a new PDF of $\text{DM}_{\text{host}}^{\text{direct}}$ for each galaxy host in our sample, from which we use the median value as our $\text{DM}_{\text{host}}^{\text{direct}}$ estimation, and 1σ for its uncertainties. For the calculation of $\text{DM}_{\text{host}}^{\text{direct}}$ we use $\text{DM}_{\text{host}}^{\text{ISM,local}}$. We note that in two cases (FRB20190611B and FRB20210117), the local H α emission line was not detected (upper limits in Table 3). However, these upper limits imply $\text{DM}_{\text{host}}^{\text{ISM}}$ values comparable with those inferred from the global measurements (Figure 2). Given that our systematic uncertainties in $\text{DM}_{\text{host}}^{\text{ISM}}$ are much larger than these differences (see below), for simplicity in the following we treat these upper limits as actual measurements.

The systematic uncertainties of changing the values of the parameters in Equation 6 are not taken into account for our reported values. For reference, these can make the $\text{DM}_{\text{host}}^{\text{ISM}}$ up to 2 (3) times larger (smaller) than our fiducial values (see also Section 4.5). Similarly, the systematic uncertainty from the chosen path length, either in the ISM or in the halo, can make $\text{DM}_{\text{halo}}^{\text{halo}}/\text{DM}_{\text{halo}}^{\text{halo}}$ up to 1.4 or 2 times larger respectively, while in the case of the FRB being in the outskirts of the halo (unlikely given the known projected distance distributions), both these contributions could be as small as zero.

3.2. Estimating DM_{host} with the Macquart Relation

For comparison, we also provide an indirect estimation of DM_{host} referred to as $\text{DM}_{\text{host}}^{\text{Macquart}}$ (rest-frame) using the follow equation:

$$\text{DM}_{\text{host}}^{\text{Macquart}} = (1+z)(\text{DM}_{\text{FRB}} - \text{DM}_{\text{MW}} - \langle \text{DM}_{\text{cosmic}} \rangle) \quad (10)$$

where $\langle \text{DM}_{\text{cosmic}} \rangle$ is the average contribution of extragalactic gas at redshift z . This analysis requires estimations of DM_{MW} and $\text{DM}_{\text{cosmic}}$.

3.2.1. DM_{MW} contribution

The Milky Way contribution comes from the ISM and the halo (Equation 3). For $\text{DM}_{\text{MW}}^{\text{ISM}}$, we use the NE2001 model (Cordes et al. 2003), where the free electrons are integrated across the Galaxy according to the FRB coordinates. NE2001 is a Galactic distribution model of free electrons which actually comprises

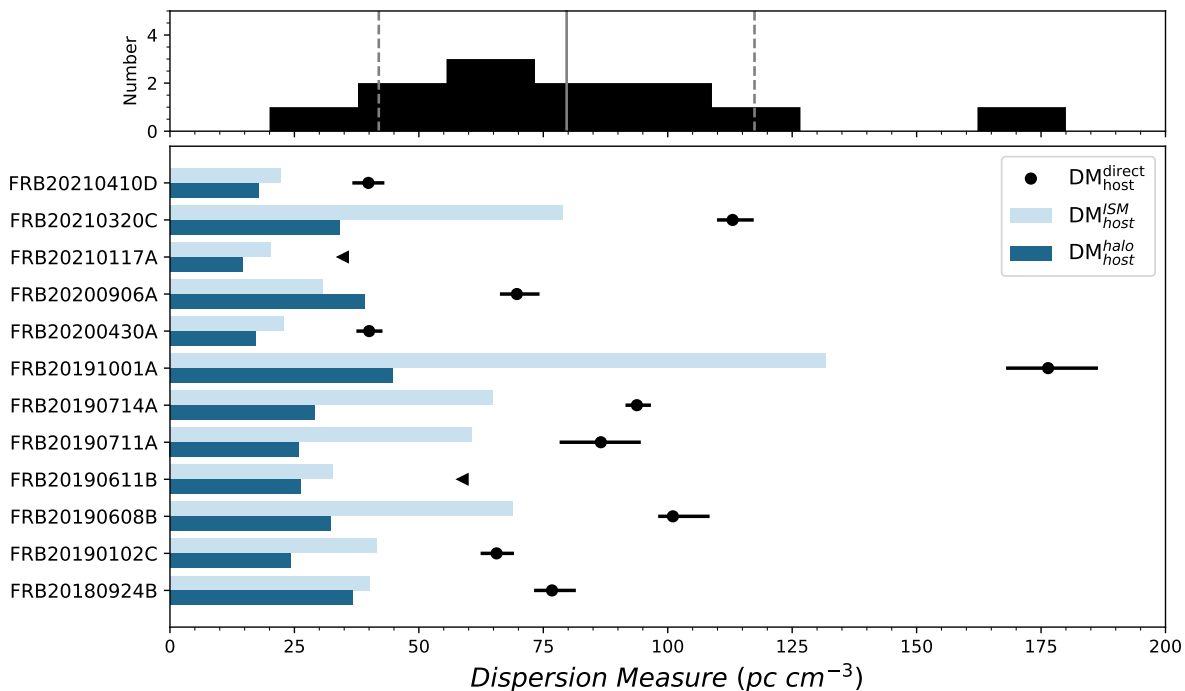


Fig. 4. Estimates of DM_{host} for the 12 FRB hosts, which shows our empirical direct estimate $DM_{\text{host}}^{\text{direct}}$ (black points). The main panel shows each contribution of $DM_{\text{host}}^{\text{direct}}$, $DM_{\text{host}}^{\text{halo}}$ in dark blue bars and $DM_{\text{host}}^{\text{ISM}}$ in light-blue bars. The upper panel is the histogram for $DM_{\text{host}}^{\text{direct}}$ where the mean and the standard deviation ($\pm 1\sigma$) of the distribution are represented by the solid and dashed vertical lines, respectively.

two disk components: spiral arms, and localized regions (like the Magellanic Clouds). For $DM_{\text{MW}}^{\text{halo}}$, we use a fixed value of 40 pc cm^{-3} (Prochaska & Zheng 2019).

3.2.2. $DM_{\text{host}}^{\text{Macquart}}$ and upper limit on DM_{host}

Given our estimates of DM_{MW} for each FRB sightline, and $\langle DM_{\text{cosmic}} \rangle$ for an average sightline up to redshift $z = z_{\text{frb}}$ (given by ΛCDM), we use Equation 10 to obtain the predicted Macquart DM_{host} , $DM_{\text{host}}^{\text{Macquart}}$. We note that for two cases this $DM_{\text{host}}^{\text{Macquart}}$ results in a negative (non-physical) value; we nevertheless report them as such for the sake of completeness and for statistical consistency (see Section 4).

We caution the reader that every sightline is unique, and thus we expect deviations from $\langle DM_{\text{cosmic}} \rangle$ for individual FRBs with the majority of DM_{cosmic} expected to lie below this value (e.g. Baptista et al. 2024). This in turn implies that our $DM_{\text{host}}^{\text{Macquart}}$ value will most of the time be an underestimation of the true DM_{host} , while the rest of the time an overestimation. However, we expect that the average $DM_{\text{host}}^{\text{Macquart}}$ value of the ensemble of measurements to be close to the average true DM_{host} value of the ensemble, modulo systematic errors e.g. in DM_{MW} .

We use the same principle to estimate a maximum possible value of DM_{host} (rest-frame), referred to as $DM_{\text{host}}^{\text{max}}$, for a given individual FRB, following:

$$DM_{\text{host}}^{\text{max}} = (1 + z)(DM_{\text{FRB}} - DM_{\text{MW}}^{\text{min}} - DM_{\text{cosmic}}^{\text{min}}), \quad (11)$$

where $DM_{\text{MW}}^{\text{min}}$ is the minimum possible value for DM_{MW} allowed by the NE2001 model, and $DM_{\text{cosmic}}^{\text{min}}$ being a conservative minimum contribution to DM_{FRB} by the IGM. For this, we use

the lower 1% percentile of the allowed scatter around the Macquart relation, that is, assuming that the FRB traveled through an extremely under-dense sightline, without intersecting any dense cosmic web filament nor intervening halos of galaxies. Although it is very unlikely to observe such an extreme situation in a sample of only 12 FRBs, we use this estimation to provide a conservative upper limit for the DM_{host} .

4. Results and Discussion

Our results on $DM_{\text{host}}^{\text{direct}}$ are shown in Figure 4 and summarized in Tables 3 and 4. We have found that on average $\langle DM_{\text{host}} \rangle = 80 \pm 11 \text{ pc cm}^{-3}$ with a standard deviation of the $DM_{\text{host}}^{\text{direct}}$ distribution of 38 pc cm^{-3} . This value is larger than the typically used value of 50 pc cm^{-3} (Arcus et al. 2020) but consistent within uncertainties. In the following we investigate possible correlations of the individual $DM_{\text{host}}^{\text{direct}}$ values as a function of galaxy properties including redshift, and also investigate the impact of possible systematic biases present in our current estimates.

4.1. Comparison between $DM_{\text{host}}^{\text{direct}}$ and $DM_{\text{host}}^{\text{Macquart}}$

Figure 5 shows a comparison between our $DM_{\text{host}}^{\text{direct}}$ measurements and the DM_{host} expectation from the Macquart relation, $DM_{\text{host}}^{\text{Macquart}}$ (dark points). The figure also shows their corresponding average values of the ensemble (golden star): $\langle DM_{\text{host}}^{\text{Macquart}} \rangle = 179 \pm 54 \text{ pc cm}^{-3}$, and $\langle DM_{\text{host}}^{\text{direct}} \rangle = 80 \pm 11 \text{ pc cm}^{-3}$, with the error bars being their corresponding standard deviations (186 and 31 pc cm^{-3} , respectively).

Although individual measurements differ significantly between $DM_{\text{host}}^{\text{direct}}$ and $DM_{\text{host}}^{\text{Macquart}}$ (as expected), the average value

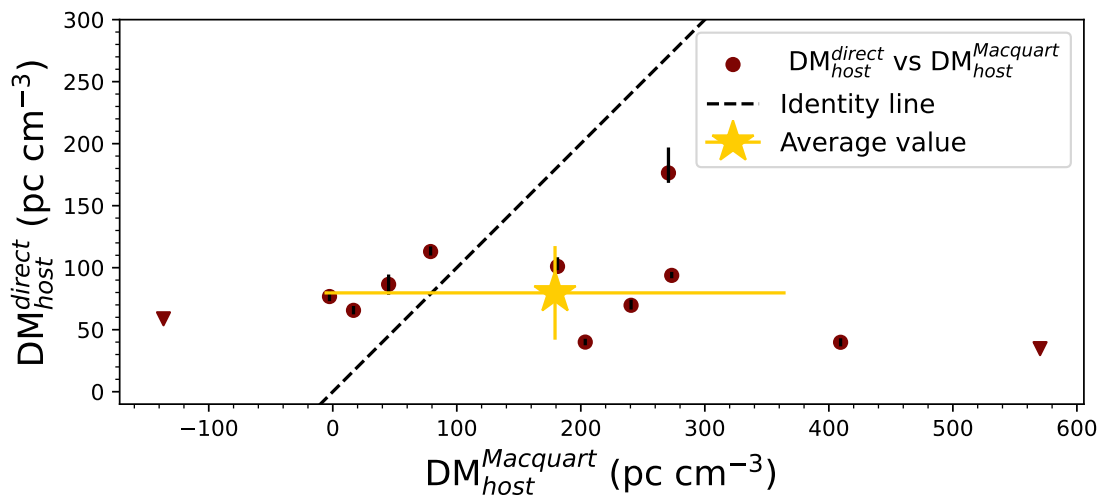


Fig. 5. Relation between $DM_{\text{host}}^{\text{direct}}$ and $DM_{\text{host}}^{\text{Macquart}}$ (dark points), with error bars showing the statistical uncertainties of $DM_{\text{host}}^{\text{direct}}$ (we do not estimate uncertainties of our $DM_{\text{host}}^{\text{Macquart}}$ values). The dashed line corresponds to the identity line (i.e. the 1:1 relation). The golden star corresponds to the average values of $DM_{\text{host}}^{\text{direct}}$ and $DM_{\text{host}}^{\text{Macquart}}$ with the error bars being their corresponding standard deviation.

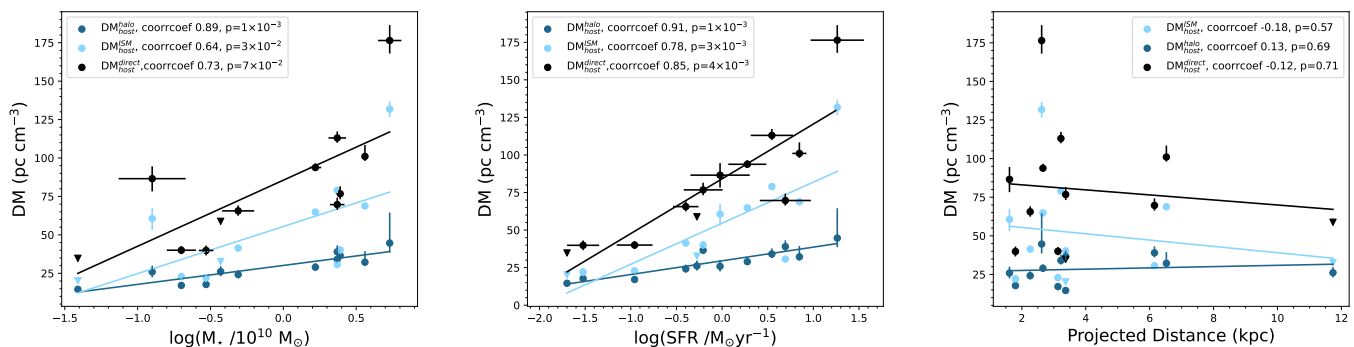


Fig. 6. Rest-frame dispersion measure (DM) as a function of stellar mass of the host (left), star-formation rate of the host (SFR; middle), and projected offset from the center of the host (right). The black points correspond to $DM_{\text{host}}^{\text{direct}}$, while the light-blue and the dark-blue points correspond to $DM_{\text{host}}^{\text{ISM}}$ and $DM_{\text{host}}^{\text{halo}}$, respectively. The black line shows a linear fit for $DM_{\text{host}}^{\text{direct}}$ ($= DM_{\text{host}}^{\text{halo}} + DM_{\text{host}}^{\text{ISM}}$), while the light-blue and dark-blue lines are the linear fits of $DM_{\text{host}}^{\text{ISM}}$ and $DM_{\text{host}}^{\text{halo}}$, respectively. The parameters of these fits are presented in Table B.1, and the Pearson coefficients and p -values are also given in the figure legends.

is consistent between them, given their statistical uncertainties. We observe that 5(7) out of 12 of our $DM_{\text{host}}^{\text{direct}}$ measurements are larger(smaller) than their corresponding $DM_{\text{host}}^{\text{Macquart}}$ values, implying that no obvious bias is present in our sample of FRBs and corresponding host galaxies for estimating the average $DM_{\text{host}}^{\text{direct}}$ (see Section 3.2). Furthermore, we observe that the scatter in $\langle DM_{\text{host}}^{\text{direct}} \rangle$ is about $\sim 5\times$ smaller than the scatter in $\langle DM_{\text{host}}^{\text{Macquart}} \rangle$ which indicates that $DM_{\text{host}}^{\text{direct}}$ may be a more precise measurement compared to $DM_{\text{host}}^{\text{Macquart}}$; however, our empirical $\langle DM_{\text{host}}^{\text{direct}} \rangle$ estimate may be subject to systematic uncertainties (of order 30%; see Section 4.5) making it (in principle) less accurate than $\langle DM_{\text{host}}^{\text{Macquart}} \rangle$. Indeed, given that mostly cosmological parameters are involved in the estimation of $DM_{\text{host}}^{\text{Macquart}}$, we only expect possible biases due to systematic errors in our individual DM_{MW}

estimates or from the stochastic effect of foreground massive halos that could contribute to the observed DM (Lee et al. 2023). Although $\langle DM_{\text{host}}^{\text{Macquart}} \rangle$ may be more accurate it is nevertheless highly uncertain, but the fact that we find consistency between $\langle DM_{\text{host}}^{\text{direct}} \rangle$ and $\langle DM_{\text{host}}^{\text{Macquart}} \rangle$ may indicate that systematic uncertainties are not dominating the measurements. Moreover, we have computed the maximum possible $DM_{\text{host}}^{\text{max}}$ given our cosmological parameters (see Section 3.2) and all our $DM_{\text{host}}^{\text{direct}}$ measurements are smaller than such a limit (see the fifth and sixth columns in Table 4), ensuring consistency.

Finally, we note that we do not see any strong correlation between $DM_{\text{host}}^{\text{direct}}$ and $DM_{\text{host}}^{\text{Macquart}}$ (Pearson coefficient of -0.2 , with p -value of 0.6) indicating that our current modeling could be missing an important DM contribution to the DM_{FRB} , i.e., some

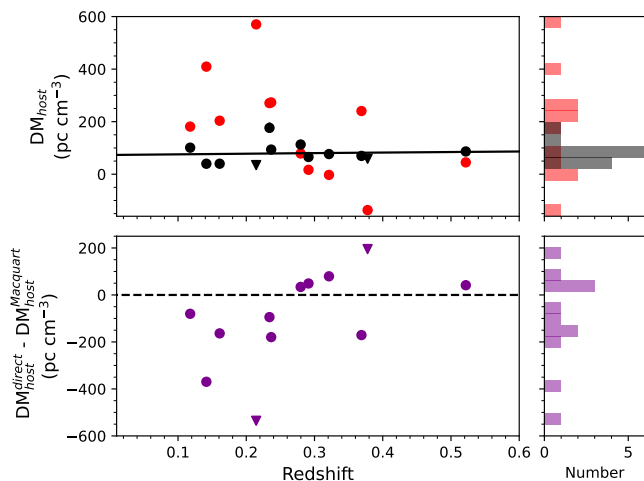


Fig. 7. Top panel: DM_{host} as a function of redshift, black and red points correspond to $DM_{\text{host}}^{\text{direct}}$ and $DM_{\text{host}}^{\text{Macquart}}$, respectively. The black line is the tendency of $DM_{\text{host}}^{\text{direct}}$. Negative values for $DM_{\text{host}}^{\text{Macquart}}$ are nonphysical; we nevertheless report them as such for statistical consistency. Histograms of the different samples are shown in the right respective panels following the same color scheme. Bottom panel: The purple points show the difference between $DM_{\text{host}}^{\text{direct}}$ and $DM_{\text{host}}^{\text{Macquart}}$ as a function of redshift. The black dashed line at value 0 indicates where $DM_{\text{host}}^{\text{direct}}$ and $DM_{\text{host}}^{\text{Macquart}}$ are equal. Histogram of the sample is shown in the right panel.

FRBs may have large intrinsic DM_{host} and/or a much larger actual DM_{cosmic} compared to the $\langle DM_{\text{cosmic}} \rangle$ (e.g. due to intervening foreground structures) that our modeling is not capturing or taken in consideration. Indeed, the apparent lack of correlation between the two estimates is partially driven by the two data-points with the largest $DM_{\text{host}}^{\text{Macquart}}$.

4.2. Correlations between $DM_{\text{host}}^{\text{direct}}$ and galaxy properties

The left panel of Figure 6 compares the $DM_{\text{host}}^{\text{direct}}$ (black points) to the corresponding stellar masses of the host galaxies. We also show the individual contributions to the $DM_{\text{host}}^{\text{direct}}$ from $DM_{\text{host}}^{\text{halo}}$ (dark blue) and $DM_{\text{host}}^{\text{ISM}}$ (light blue). We observe a positive correlation between $DM_{\text{host}}^{\text{direct}}$ and stellar mass, of the form:

$$\left(\frac{DM_{\text{host}}}{\text{pc cm}^{-3}} \right) \approx 43 \log \left(\frac{M_{\star}}{10^{10} M_{\odot}} \right) + 86 \quad (12)$$

with a Pearson correlation test giving a coefficient of 0.73 (with p -value of 7×10^{-2}). A correlation of DM_{host} with stellar mass is expected, given that the larger the stellar mass, the larger the halo mass used to estimate $DM_{\text{host}}^{\text{halo}}$ (see Section 3.1.3). Indeed, we also see a positive correlation between $DM_{\text{host}}^{\text{halo}}$ and stellar mass with Pearson coefficient of 0.89 (with p -value of 1×10^{-3}). Interestingly, a positive correlation is also present between $DM_{\text{host}}^{\text{ISM}}$ and stellar mass (Pearson coefficient of 0.64, with p -value of 3×10^{-2}), which we attribute to the fact that most galaxies in our sample are star-forming and the existence of the star-formation main sequence (SFMS; e.g. Brinchmann et al. 2004; see below).

The middle panel of Figure 6 shows $DM_{\text{host}}^{\text{direct}}$ (black points) as a function of global SFR for each host galaxy; as before, the individual contributions of $DM_{\text{host}}^{\text{halo}}$ (dark blue) and $DM_{\text{host}}^{\text{ISM}}$ (light blue) are also shown. In this case we also observe a positive cor-

relation between $DM_{\text{host}}^{\text{direct}}$ (and its components) and global SFR of the form:

$$\left(\frac{DM_{\text{host}}}{\text{pc cm}^{-3}} \right) \approx 36 \log \left(\frac{\text{SFR}}{M_{\odot} \text{ yr}^{-1}} \right) + 84 \quad (13)$$

with a Pearson correlation test giving a coefficient of 0.85 (with p -value of 4×10^{-3}). A correlation with SFR could be expected given that galaxies with higher star formation activity should also have larger $S(H\alpha)$, which is directly proportional to $DM_{\text{host}}^{\text{ISM}}$ in our estimations (Equations 5 and 6). Indeed, despite the fact that we use local values of $S(H\alpha)$ to estimate $DM_{\text{host}}^{\text{ISM}}$, we have shown that for our sample both local and global values of $S(H\alpha)$ are similar (see Figure 2; see also Section 4.5). We also observe a positive correlation between $DM_{\text{host}}^{\text{halo}}$ and SFR (Pearson coefficient 0.91, with p -value of 1×10^{-3}) which can again be explained by the existence of the SFMS for star-forming galaxies.

In order to investigate whether the correlations between $DM_{\text{host}}^{\text{ISM}}$ and stellar mass, and $DM_{\text{host}}^{\text{halo}}$ and SFR are driven by the SFMS we have performed the following experiment. We used the nominal stellar mass values of the galaxies in our sample (without considering uncertainties) and obtained values for their SFR assuming they lie right on top of the SFMS fit reported by Chang et al. (2015) in their equation 4. From these, we obtained an expectation of the $H\alpha$ flux using equation 14 from Pflamm-Altenburg et al. (2007), from which we got an ‘expected’ $DM_{\text{host}}^{\text{ISM}}$ given the new $S(H\alpha)$, and by following our methodology (Section 3.1.1) but for a global measurement rather than a local measurement (see also Section 3.1.2). From such an experiment we find a correlation between $DM_{\text{host}}^{\text{ISM}}$ and $DM_{\text{host}}^{\text{halo}}$ that is stronger than our actual case (using the actual local $H\alpha$ measurements) and also stronger when we compare it with our actual global measurements. This indicates that indeed, the SFMS can account for all the correlation observed between $DM_{\text{host}}^{\text{ISM}}$ and $DM_{\text{host}}^{\text{halo}}$, and hence both $DM_{\text{host}}^{\text{ISM}}$ and stellar mass, and $DM_{\text{host}}^{\text{halo}}$ and SFR.

Finally, we also explore a possible correlation of $DM_{\text{host}}^{\text{direct}}$ with the projected distance of the FRB sightline with respect to the galaxy halo center. In the right of Figure 6 we show $DM_{\text{host}}^{\text{direct}}$ as a function of the projected distance of the FRB sightline to the center of their host galaxy (black points), again also showing their $DM_{\text{host}}^{\text{halo}}$ (dark blue points) and $DM_{\text{host}}^{\text{ISM}}$ (light blue points) contributions. In contrast to previous cases, we do not observe any strong correlation between $DM_{\text{host}}^{\text{direct}}$ and FRB projected distances (we only report a weak anti-correlation) which can be explained by the fact that the most (least) massive galaxies have their FRBs farther (closer) to their centers. This result is driven by the adopted mNFW profiles which produce a rather flat (weak anti-correlation) between $DM_{\text{host}}^{\text{halo}}$ and projected distance (see Prochaska & Zheng 2019). Furthermore, the fact that FRBs tend to lie well within the center of the dark matter halos of their host galaxies indicate that the $DM_{\text{host}}^{\text{halo}}$ is indeed dominated by the halo mass (i.e. stellar mass) rather than projected distance.

Table B.1 in the Appendix summarizes the parameters of our fits and correlation coefficients discussed in this section.

4.3. Possible redshift evolution of $DM_{\text{host}}^{\text{direct}}$ and redshift biases

We also investigate a possible redshift dependence in our DM_{host} estimates. Figure 7 shows DM_{host} as a function of redshift (top panel), where the black and red points correspond to $DM_{\text{host}}^{\text{direct}}$ and $DM_{\text{host}}^{\text{Macquart}}$, respectively. We observe no strong redshift evolution

in the individual values of DM_{host} . The black line corresponds to a fit of the form,

$$DM_{\text{host}}^{\text{direct}}(z) = DM_{\text{host},0}(1+z)^\alpha, \quad (14)$$

which shows a flat exponent ($\alpha \approx 0.3 \pm 1.7$) and a $DM_{\text{host},0} \approx 73 \pm 33 \text{ pc cm}^{-3}$, consistent with our $\langle DM_{\text{host}}^{\text{direct}} \rangle$. The apparent lack of redshift evolution indicates that DM_{host} is driven by internal galaxy properties (e.g. stellar mass and SFR) and thus no extra corrections for redshift (galaxy evolution) are needed, at least for $z \lesssim 0.5$. We remind the reader that this DM_{host} estimate is in the rest-frame, thus a factor of $(1+z)$ should still be applied when considering $DM_{\text{host}}^{\text{obs}}$ (see Equation 2).

In contrast, the $DM_{\text{host}}^{\text{Macquart}}$ estimations show a much larger scatter and a possible evolution with redshift, which may indicate a possible redshift bias. The bottom panel of Figure 7 shows the difference between $DM_{\text{host}}^{\text{direct}}$ and $DM_{\text{host}}^{\text{Macquart}}$ as a function of redshift. Here, we also observe a possible bias as a function of redshift for individual measurements where $DM_{\text{host}}^{\text{Macquart}}$ tend to be larger than our $DM_{\text{host}}^{\text{direct}}$ at lower redshifts ($z \lesssim 0.3$), and lower than $DM_{\text{host}}^{\text{direct}}$ at higher redshifts ($z \gtrsim 0.3$). This discrepancy could be due to an underestimation of the Macquart relation at lower redshifts, making $DM_{\text{host}}^{\text{Macquart}}$ systematically larger (see Equation 11). Another possibility is that our calculation of $DM_{\text{host}}^{\text{direct}}$ is underestimated at lower redshifts, caused by an unknown systematic effect; we note that the expected systematic error of $\sim 30\%$ (see Section 4.5) is not enough to make this apparent redshift bias disappear. Given that our sample size is still small, there is also the possibility of this being driven by low number statistics (e.g. the current trend is partially induced by the two FRBs with the largest $DM_{\text{host}}^{\text{Macquart}}$, which also correspond to the two largest values of DM_{FRB}), motivating future similar studies with larger samples.

4.4. Comparison with previous work

Our empirical estimation is consistent with recent observational results from Khrykin et al. (2024b) who reported $\langle DM_{\text{host}} \rangle = 90^{+29}_{-19} \text{ pc cm}^{-3}$ applied to a sample of 8 FRB sightlines and using a different methodology. However, we note that 6 out of 8 of these were also included in our analysis, and thus these two results are not fully independent. Our empirical estimation is also consistent with that of Shin et al. (2023) who reported a median value of $DM_{\text{host}} = 84^{+69}_{-49} \text{ pc cm}^{-3}$ for CHIME FRBs. In contrast, our results are inconsistent with those from Wang & van Leeuwen (2024) who reported much larger values of $\langle DM_{\text{host}} \rangle = 560^{+37}_{-190} \text{ pc cm}^{-3}$ for their power law density model, and $\langle DM_{\text{host}} \rangle = 490^{+74}_{-129} \text{ pc cm}^{-3}$ for their SFR model, also for CHIME FRBs. Our estimates are also lower than those reported by Bhardwaj et al. (2024) based on FRB scattering timescales, of $\langle DM_{\text{host}} \rangle \gtrsim 170 \text{ pc cm}^{-3}$ for a range of galaxy inclinations.

In terms of recent theoretical work, Mo et al. (2023) analyzed cosmological hydrodynamical simulations using two different models for the location of FRBs within the simulated host galaxies: (i) following the star-formation, and (ii) following the stellar mass. They obtained different DM_{host} values for these different models, reporting medians of 179 and 63 pc cm^{-3} (rest-frame), respectively. Our observational result lies between these two values, and is consistent with both of them given the reported uncertainties and large scatter across models. Mo et al. (2023) also report a linear relation between their inferred DM_{host} and the logarithm of the host stellar mass for both models following a

similar trend as the one reported here, although again with much larger variations depending on the model used (see also Zhang et al. 2020; Kovacs et al. 2024). Finally they report a possible evolution of DM_{host} (rest-frame) with redshift using a power-law fit as we do here (Equation 14), but with an α varying between 0.8 and 1.8 depending on the model (see also Zhang et al. 2020; Kovacs et al. 2024; Orr et al. 2024), whereas we do not see any evolution from our current sample (see Section 4.3). Therefore, empirical DM_{host} estimations have the potential to constrain sub-grid physics of galaxy evolution (e.g. Khrykin et al. 2024b) and also provide important clues for the origin of FRBs themselves.

4.5. Systematic uncertainties

In this work we model $DM_{\text{host}}^{\text{direct}}$ as the sum of two contributions: $DM_{\text{host}}^{\text{ISM}}$ and $DM_{\text{host}}^{\text{halo}}$ (see Section 3.1). Out of these two estimates, we consider that $DM_{\text{host}}^{\text{ISM}}$ is more uncertain than $DM_{\text{host}}^{\text{halo}}$ because of the several assumptions regarding geometry, temperature, and other properties of the interstellar medium, and such systematic effects are not fully accounted for in our reported statistical uncertainties; for instance, recent studies of pulsars in the Large Magellanic Cloud (LMC), report variations of observed DMs of several tens of pc cm^{-3} (e.g. Prayag et al. 2024, see their table 1). In a more extreme situation, if FRBs originate outside the disks of galaxies (e.g. globular clusters; Kirsten et al. 2022), then $DM_{\text{host}}^{\text{ISM}} \sim 0 \text{ pc cm}^{-3}$, at least for those cases in which the FRB is foreground to the disk itself. Although the $DM_{\text{host}}^{\text{halo}}$ inferences also depend on several systematic factors, including the assumed model of baryons around galaxies (Equation 9), ionization fraction (f_{ion}) and the path length of the FRB along the galaxy host halo, the fact that we sample $DM_{\text{host}}^{\text{halo}}$ from a PDF that does include (already large) uncertainties in both the stellar mass and the dark matter halo mass, makes their systematic effect less important relative to those associated with $DM_{\text{host}}^{\text{ISM}}$.

In order to estimate such a systematic effect we have repeated our individual $DM_{\text{host}}^{\text{direct}}$ measurements using 10^5 realizations of $DM_{\text{host}}^{\text{ISM}}$ uniformly sampled from a PDF whose mean value is between [0.5, 1.5] times our fiducial values (e.g. those reported in Table 3, sixth column), leaving $DM_{\text{host}}^{\text{halo}}$ unchanged (see Section 3.1.4 and Equation 4). We consider that such a range in variation includes most of the systematic uncertainties in $DM_{\text{host}}^{\text{ISM}}$ (including geometrical factors that appear in Equation 6). Figure C.1 in the Appendix shows the effect of this experiment in our $DM_{\text{host}}^{\text{direct}}$ measurement, where the shaded orange region represents the 1σ uncertainty (systematic) around our fiducial trends, corresponding to a $\sim 30\%$ (systematic) impact on $DM_{\text{host}}^{\text{direct}}$.

In the context of measuring $DM_{\text{host}}^{\text{ISM}}$, one can consider both a global or local measurement of $S(\text{H}\alpha)$ (see Section 3.1.2). In our sample we have empirically found that both give quite similar results (see Figure 2) given their statistical uncertainties. Such a result is partly driven by some of our galaxies not being fully resolved (7 out of the 12 have half-light radii comparable with the $0.4''$ radius used for our local measurement). Similarly, we find that the larger differences between the two are coming from FRBs that have larger projected distances with respect to the disks traced by $\text{H}\alpha$ (as expected), but these cases are a minority (namely FRB20190611B and FRB20210117A). In other words, most of the FRBs in our sample are coming from galaxy disks (e.g. Mannings et al. 2021). The systematic difference between the two is small and only implies a $\approx 14\%$ bias in $DM_{\text{host}}^{\text{ISM}}$, which is already contained in the $\sim 30\%$ systematic uncertainty budget reported above. Therefore, we conclude that estimating

$DM_{\text{host}}^{\text{ISM}}$ from a global $H\alpha$ measurement provides similar level of accuracy than using a local estimate for partially resolved galaxies. This is not to say that both are the same, but just an observational limitation of our adopted technique. Finally, considering a more extreme (yet unlikely) situation where $DM_{\text{host}}^{\text{ISM}} = 0 \text{ pc cm}^{-3}$, then only our results for $DM_{\text{host}}^{\text{halo}}$ (e.g. see Table B.1) should be used as reference for $DM_{\text{host}}^{\text{direct}}$ instead.

Postgrado PUCV 2022-2023. ISK and NT acknowledge the support received by the Joint Committee ESO-Government of Chile grant ORP 40/2022. LBC, NT, ISK, and JXP, as members of the Fast and Fortunate for FRB Follow-up team, acknowledge support from NSF grants AST-1911140, AST-1910471 and AST-2206490. LM is supported by an Australian Government Research Training Program (RTP) Scholarship. RMS acknowledges support through Australian Research Council Future Fellowship FT190100155 and Discovery Project DP220102305.

5. Summary and Conclusions

In this work, we have empirically estimated the dispersion measure of FRB host galaxies, DM_{host} , using a sample of 12 well-localized FRBs at redshifts $0.11 < z < 0.53$ observed with VLT/MUSE. For this estimation, we employ a method that considers the stellar mass of the host galaxies and the projected distance to the FRBs in order to infer the contribution from the host halos, $DM_{\text{host}}^{\text{halo}}$, and the $H\alpha$ nebular emission line flux to infer the contribution from their interstellar medium (ISM), $DM_{\text{host}}^{\text{ISM}}$. The sum of these two contributions is our direct estimation of DM_{host} , referred to as $DM_{\text{host}}^{\text{direct}}$ (see Equation 4). For comparison purposes we also estimate the inferred DM_{host} , assuming that the sightlines to the FRBs have an intergalactic medium DM contribution given by the Macquart relation, referred to as $DM_{\text{host}}^{\text{Macquart}}$ (see Equation 10). We summarize our main results as follows:

1. We find that on average $\langle DM_{\text{host}} \rangle = 80 \pm 11 \text{ pc cm}^{-3}$ with a standard deviation of 38 pc cm^{-3} (the uncertainty here is only statistical). We have estimated a systematic uncertainty of $\sim 30\%$ in our results, driven mostly by the unknown physical properties of the host ISM gas through which the FRB pulse propagated (including the immediate environment around the progenitor). Our reported $DM_{\text{host}}^{\text{direct}}$ is larger than the typically used (fixed) value of 50 pc cm^{-3} but consistent within uncertainties.
2. We find no strong correlation between $DM_{\text{host}}^{\text{direct}}$ and $DM_{\text{host}}^{\text{Macquart}}$, indicating that our current modeling could be missing an important DM contribution to the DM_{FRB} for a fraction of FRBs (e.g. intrinsic variations to DM_{host} and/or unaccounted intervening halos or cosmic web structures).
3. We find a positive correlation between $DM_{\text{host}}^{\text{direct}}$ with stellar mass and SFR of the host galaxy (see Figure 6) of the form given by Equations 12 and 13 (parameters summarized in Table B.1). In contrast, no strong correlation is observed between $DM_{\text{host}}^{\text{direct}}$ and FRB projected distance with respect to the host centers (see Section 4.2).
4. We do not find any strong redshift evolution of DM_{host} (rest-frame) in our sample (Figure 7 and Section 4.3). However, we find a possible redshift bias associated with the indirect estimation of DM_{host} based on the Macquart relation, and/or produced by an unknown bias in our $DM_{\text{host}}^{\text{direct}}$ measurements.

Our reported correlations and the lack of a strong redshift evolution can be used to constrain models for the progenitor of FRBs, e.g. by comparing them with theoretical models. However, larger samples are needed to keep improving on the present results and thus provide more precise and accurate observed values of DM_{host} .

Acknowledgements. We thank the anonymous referee for their careful revision and suggestions that improved the paper. We thank Ron Ekers and Kasper Heintz for useful comments and discussions. This work is based on observations collected at the European Southern Observatory under ESO programmes 2102.A-5005, 0104.A-0411, 0105.20HG and 0110.241Y. LBC and NT acknowledge support by FONDECYT grant 11191217. LBC acknowledge support by Beca

FRB name	$H\alpha^{local}$ (10^{-18} erg s $^{-1}$ cm $^{-2}$)	$H\alpha^{global}$ (10^{-18} erg s $^{-1}$ cm $^{-2}$)	$S(H\alpha)^{local}$ (10^{-18} erg s $^{-1}$ cm $^{-2}$ arcsec $^{-2}$)	$S(H\alpha)^{global}$ (10^{-18} erg s $^{-1}$ cm $^{-2}$ arcsec $^{-2}$)	$DM_{host}^{ISM,local}$ (pc cm $^{-3}$)	$DM_{host}^{ISM,global}$ (pc cm $^{-3}$)
(1)	(2)	(3)	(4)	(5)	(6)	(7)
FRB20180924B	21.6±3.0	104.1±13.5	154.8±21.3	316.5±42.2	40.2±2.7	57.3±4.3
FRB20190102C	20.7±2.2	59.3±16.3	157.2±16.9	103.2±27.5	41.4±2.2	33.7±4.3
FRB20190608B	106.8±5.2	5292.8±525.7	325.3±15.9	350.6±34.8	68.8±1.7	71.5±3.4
FRB20190611B	<8.8 †	23.0±5.3	<111.3 †	245.8±56.3	<32.7 †	48.6±5.5
FRB20190711A	34.8±8.2	16.1±16.6	467.9±110.3	313.5±323.6	60.6±7.6	51.3±17.3
FRB20190714A	70.0±2.4	524.4±68.0	353.1±12.1	498.6±64.6	64.8±1.1	77.0±4.8
FRB20191001A	309.0±25.2	1765.6±261.9	1453.1±118.4	1173.4±174.1	131.8±5.2	118.3±8.5
FRB20200430A	11.1±1.9	168.2±13.2	38.9±6.7	197.2±15.5	22.9±1.9	51.6±2.2
FRB20200906A	11.1±1.3	686.4±114.3	97.0±11.1	436.7±72.7	30.7±1.7	64.9±5.1
FRB20210117A	<7.1 †	20.1±4.7	<32.9 †	27.6±6.4	<20.1 †	18.5±1.9
FRB20210320C	78.6±3.7	805.0±77.0	561.4±26.2	602.4±57.6	79.0±1.8	81.7±4.0
FRB20210410D	7.6±2.1	53.9±8.1	35.1±9.6	134.7±20.3	22.1±2.8	43.4±2.9

Table 3. Road to DM_{host}^{ISM} . (1) Name of the FRB; (2) Local $H\alpha$ flux from MUSE cubes (see Section 3.1.1); (3) Global $H\alpha$ flux from MUSE cubes; (4) Local $H\alpha$ surface brightness, corrected for dust extinction and brightness dimming; (5) Global $H\alpha$ surface brightness; (6) Local ISM Dispersion Measure; (7) Global ISM Dispersion Measure.

† : Non-detections are reported as 2σ upper limits.

FRB name	$\log(M_{\star} / M_{\odot})$	$\log(M_{halo} / M_{\odot})$	DM_{host}^{halo} (pc cm $^{-3}$)	DM_{host}^{direct} (pc cm $^{-3}$)	DM_{host}^{max} (pc cm $^{-3}$)	$DM_{host}^{Macquart, \dagger}$ (pc cm $^{-3}$)
(1)	(2)	(3)	(4)	(5)	(6)	(7)
FRB20180924B	10.39±0.02	11.96±0.1	36±3	76±4	167	-2
FRB20190102C	9.69±0.09	11.47±0.14	24±2	65±3	169	16
FRB20190608B	10.56±0.02	12.09±0.11	32±7	101±7	241	181
FRB20190611B	9.57±0.12	11.43±0.15	26±3	58±4	67	-136
FRB20190711A	9.10±0.15	11.23±0.2	25±4	86±8	332	34
FRB20190714A	10.22±0.04	11.79±0.1	28±2	93±2	394	273
FRB20191001A	10.73±0.07	12.37±0.21	44±19	176±20	391	270
FRB20200430A	9.30±0.07	11.22±0.14	17±2	40±2	285	203
FRB20200906A	10.37±0.05	11.96±0.11	38±4	69±4	438	240
FRB20210117A	8.59±0.05	10.91±0.15	14±1	34±2	678	569
FRB20210320C	10.37±0.05	11.93±0.11	34±3	113±4	224	78
FRB20210410D	9.47±0.05	11.29±0.13	17±1	39±3	481	409

Table 4. Summary of our main results (including road to DM_{host}^{halo}). (1) Name of the FRB; (2) Stellar mass of host galaxy; (3) Halo mass of host galaxy (see Section 3.1.3); (4) Dispersion measure of the halo of the host galaxy (see Section 3.1.3); (5) Empirical dispersion measure of the host galaxy (our main result; see Section 3.1.4); (6) Upper limit for the dispersion measure of the host galaxy (see Section 3.2); (7) Average dispersion measure of the host galaxy estimated from the Macquart relation (see Section 3.2).

† : Although negative values are nonphysical, we nevertheless report them as such for statistical consistency when taking the average of the ensemble.

Appendix A: H α emission for the rest of the sample

In Figures A.1 to A.11 we show, as in Figure 1 the location of the FRB within the host galaxy, along with the corresponding extracted spectrum for the rest of the sample, excluding FRB20191001A shown already in Figure 1. The galaxy map corresponds to the measured emission line (H α , H β , H γ , as appropriate).

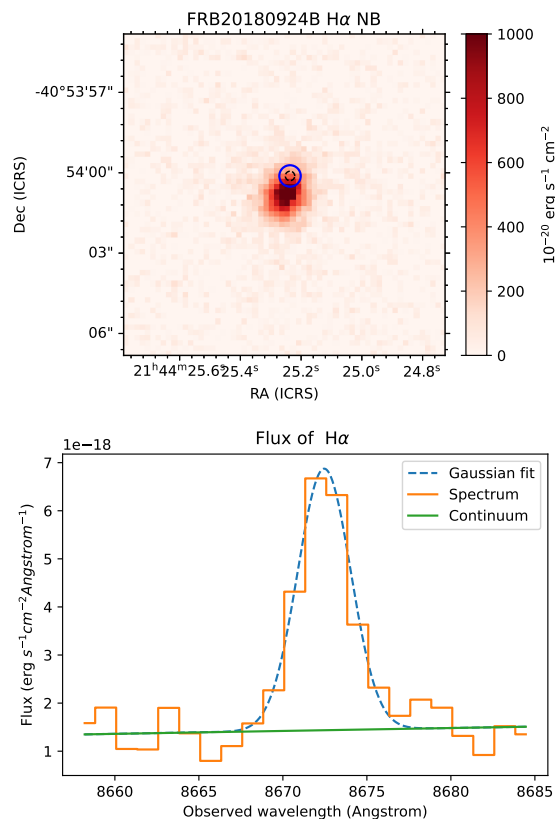


Fig. A.1. Same as Figure 1 but for FRB20180924B.

Appendix C: Systematic uncertainty estimation of our reported trends

In Figure C.1 we show our estimated systematic uncertainties (shaded brown regions) for the different reported trends of Section 4.2. Details on how this is done are given in Section 4.5.

References

- Aggarwal, K., Budavári, T., Deller, A. T., et al. 2021, *ApJ*, 911, 95
- Arcus, W. R., Macquart, J. P., Sammons, M. W., James, C. W., & Ekers, R. D. 2020, *MNRAS*, 000, 1
- Bacon, R., Accardo, M., Adjali, L., et al. 2010, in *Ground-based and Airborne Instrumentation for Astronomy III*, Vol. 7735 (SPIE), 773508
- Bannister, K. W., Deller, A. T., Phillips, C., et al. 2019, *Science*, 365, 565
- Baptista, J., Prochaska, J. X., Mannings, A. G., et al. 2024, *ApJ*, 965, 57
- Bhandari, S., Bannister, K. W., Lenc, E., et al. 2020, *The Astrophysical Journal Letters*, 901, L20
- Bhandari, S., Gordon, A. C., Scott, D. R., et al. 2023, *ApJ*, 948, 67
- Bhandari, S., Heintz, K. E., Aggarwal, K., et al. 2022, *AJ*, 163, 69
- Bhardwaj, M., Lee, J., & Ji, K. 2024, *Nature*, 634, 1065
- Brinchmann, J., Charlot, S., White, S. D. M., et al. 2004, *MNRAS*, 351, 1151
- Caleb, M., Driessen, L. N., Gordon, A. C., et al. 2023, *MNRAS*[arXiv:2302.09754]
- Calzetti, D., Armus, L., Bohlin, R. C., et al. 2000, *ApJ*, 533, 682
- Chang, Y.-Y., van der Wel, A., da Cunha, E., & Rix, H.-W. 2015, *ApJS*, 219, 8
- Chittidi, J. S., Simha, S., Mannings, A., et al. 2020, *The Astrophysical Journal*, 922, 173
- Cordes, J. M. & Chatterjee, S. 2019, *ARA&A*, 57, 417
- Cordes, J. M., Joseph, T., & Lazio, W. 2003, arXiv e-prints, arXiv:astro
- Cordes, J. M., Wharton, R. S., Spitler, L. G., Chatterjee, S., & Wasserman, I. 2016, arXiv e-prints, arXiv:1605.05890
- Dall’Osso, S., La Placa, R., Stella, L., Bakala, P., & Possenti, A. 2024, arXiv e-prints, arXiv:2407.04095
- Day, C. K., Deller, A. T., Shannon, R. M., et al. 2020, *Monthly Notices of the Royal Astronomical Society*, 497, 3335
- ESO CPL Development Team. 2015, *EsoRex: ESO Recipe Execution Tool*, Astrophysics Source Code Library, record ascl:1504.003

Appendix B: Parameters of the reported fits

In Table B.1 we present a summary of the parameters reported in our fits of Section 4.2 .

Component y	M_{\star}				SFR				Offset			
	b (pc cm^{-3})	m	Pearson coeff.	p value	b (pc cm^{-3})	m	Pearson coeff.	p value	b (pc cm^{-3})	m	Pearson coeff.	p value
(1)	(2)				(3)				(4)			
DM _{host} ^{direct}	86±8	43±13	0.73	7×10 ⁻²	84±5	36±7	0.85	4×10 ⁻³	86±21	-2±4	0.22	0.71
DM _{host} ^{halo}	30±1	12±2	0.89	1×10 ⁻³	30±1	9±1	0.91	1×10 ⁻³	26±5	0±1	0.13	0.69
DM _{host} ^{ISM}	55±8	31±12	0.64	3×10 ⁻²	55±6	27±7	0.78	3×10 ⁻³	60±14	-2±3	-0.18	0.57

Table B.1. Parameters of linear fits of the form $y = mx + b$ for correlations shown in Figure 6 (see also Section 4.2) and their corresponding Pearson coefficients and p -values.. (1) Component fitted; (2) Parameters for stellar mass fits, with $x = \log(M_{\star}/10^{10}M_{\odot})$; (3) Parameters for SFR fits, with $x = \log(\text{SFR}/M_{\odot}\text{yr}^{-1})$; (4) Parameters for projected distance fits, with x being the impact parameter between the FRB and the galaxy center in kpc .

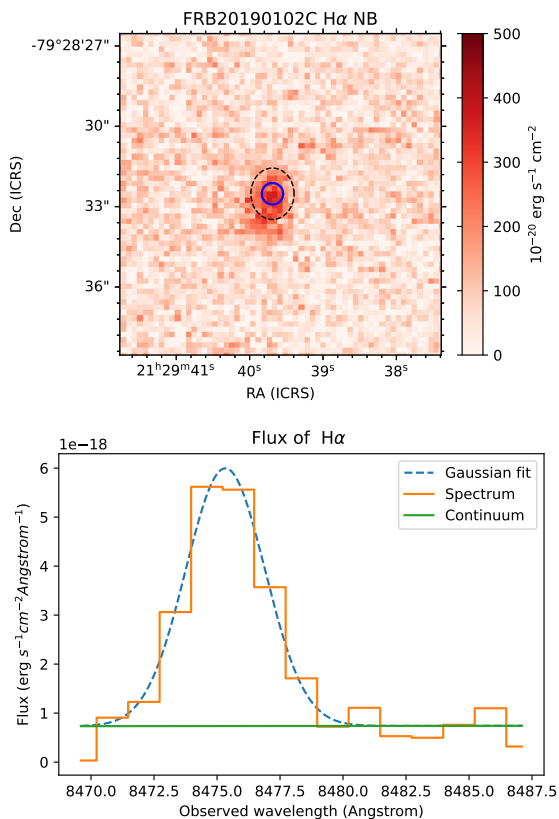


Fig. A.2. Same as Figure 1 but for FRB20190102C.

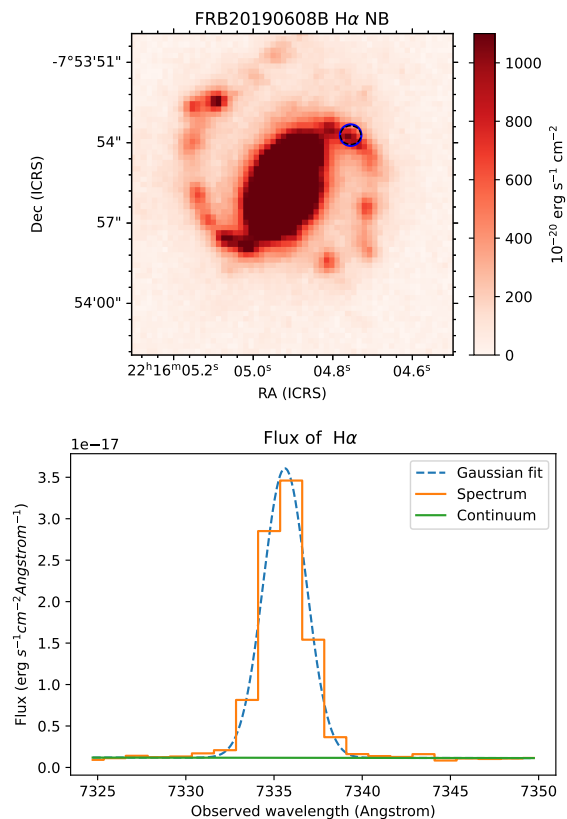


Fig. A.3. Same as Figure 1 but for FRB20190608B.

Fitzpatrick, E. L. & Massa, D. 2007, *ApJ*, 663, 320
 Gordon, A. C., Fong, W.-f., Kilpatrick, C. D., et al. 2023, *ApJ*, 954, 80
 Heintz, K. E., Xavier Prochaska, J., Simha, S., et al. 2020, Host galaxy properties and offset distributions of fast radio bursts: Implications for their progenitors
 James, C. W., Ghosh, E. M., Prochaska, J. X., et al. 2022a, *Monthly Notices of the Royal Astronomical Society*, 516, 4862
 James, C. W., Prochaska, J. X., Macquart, J. P., et al. 2022b, *MNRAS*, 509, 4775
 Khrykin, I. S., Ata, M., Lee, K.-G., et al. 2024b, *ApJ*, 973, 151
 Khrykin, I. S., Sorini, D., Lee, K.-G., & Davé, R. 2024a, *MNRAS*, 529, 537
 Kirsten, F., Marcote, B., Nimmo, K., et al. 2022, *Nature*, 602, 585
 Kovacs, T. O., Mao, S. A., Basu, A., et al. 2024, *arXiv e-prints*, arXiv:2407.16748
 Lee, K.-G., Khrykin, I. S., Simha, S., et al. 2023, *ApJ*, 954, L7
 Logroño-García, R., Vilella-Rojo, G., López-Sanjuan, C., et al. 2019, *A&A*, 622, A180
 Lorimer, D. R., Bailes, M., McLaughlin, M. A., Narkevic, D. J., & Crawford, F. 2007, *Science*, 318, 777
 Macquart, J.-P., Bailes, M., Bhat, N. D. R., et al. 2010, *Publications of the Astronomical Society of Australia*, Volume 27, Issue 3, pp. 272-282., 27, 272
 Macquart, J. P., Prochaska, J. X., McQuinn, M., et al. 2020, *Nature*, 581, 391
 Mannings, A. G., Fong, W.-f., Simha, S., et al. 2021, *ApJ*, 917, 75
 Marcote, B., Nimmo, K., Hessels, J. W., et al. 2020, *Nature*, 577, 190
 Mathews, W. G. & Prochaska, J. X. 2017, *ApJ*, 846, L24

Michilli, D., Seymour, A., Hessels, J. W. T., et al. 2018, *Nature*, 553, 182
 Mo, J.-F., Zhu, W., Wang, Y., Tang, L., & Feng, L.-L. 2023, *MNRAS*, 518, 539
 Moster, B. P., Naab, T., & White, S. D. 2013, *Monthly Notices of the Royal Astronomical Society*, 428, 3121
 Niu, C. H., Aggarwal, K., Li, D., et al. 2022, *Nature*, 606, 873
 Orr, M. E., Burkhart, B., Lu, W., Ponnada, S. B., & Hummels, C. B. 2024, *ApJ*, 972, L26
 Osterbrock, D. E. & Ferland, G. J. 2006, *Astrophysics of gaseous nebulae and active galactic nuclei*
 Ouyed, R., Leahy, D., & Koning, N. 2020, *Research in Astronomy and Astrophysics*, 20, 027
 Petroff, E., Hessels, J. W. T., & Lorimer, D. R. 2019, *The Astronomy and Astrophysics Review*, 27, 4
 Petroff, E., Hessels, J. W. T., & Lorimer, D. R. 2022, *A&A Rev.*, 30, 2
 Pflamm-Altenburg, J., Weidner, C., & Kroupa, P. 2007, *ApJ*, 671, 1550
 Planck Collaboration, Aghanim, N., Akrami, Y., et al. 2020, *A&A*, 641, A6
 Platts, E., Weltman, A., Walters, A., et al. 2019, *Phys. Rep.*, 821, 1
 Prayag, V., Levin, L., Geyer, M., et al. 2024, *MNRAS*[arXiv:2408.04899]
 Prochaska, J. X., Simha, S., almannin, et al. 2023, FRBs/FRB: Release to sync with Gordon et al. 2023
 Prochaska, J. X. & Zheng, Y. 2019, *Monthly Notices of the Royal Astronomical Society*, 485, 648

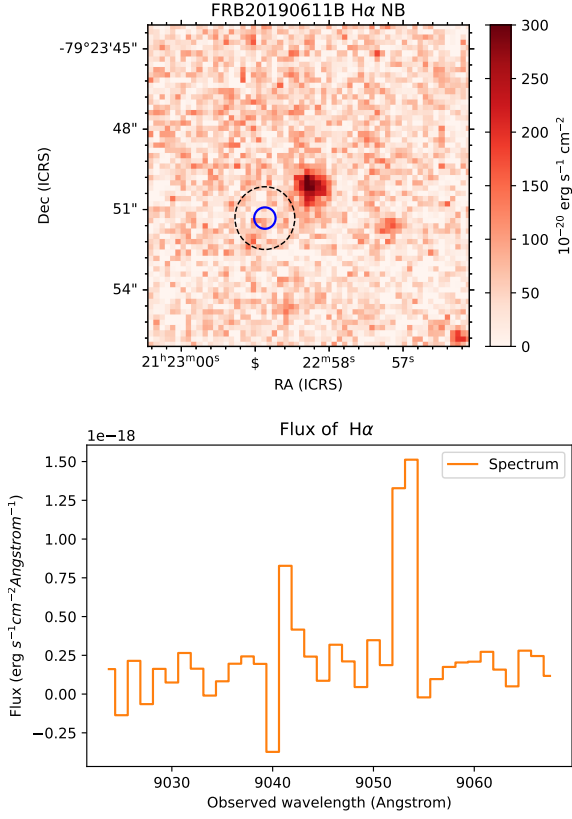


Fig. A.4. Same as Figure 1 but for FRB20190611B. In this case, we cannot fit a Gaussian and thus just report a 2σ upper limit.

- Rajwade, K. M., Bezuidenhout, M. C., Caleb, M., et al. 2022, Monthly Notices of the Royal Astronomical Society, 514, 1961
- Reynolds, R. J. 1977, 216, 433
- Shannon, R. M., Bannister, K. W., Bera, A., et al. 2024, arXiv e-prints, arXiv:2408.02083
- Shin, K., Masui, K. W., Bhardwaj, M., et al. 2023, ApJ, 944, 105
- Simha, S., Lee, K.-G., Prochaska, J. X., et al. 2023, ApJ, 954, 71
- Tendulkar, S. P., Bassa, C. G., Cordes, J. M., et al. 2017, The Astrophysical Journal, 834, L7
- Wang, Y. & van Leeuwen, J. 2024, A&A, 690, A377
- Weilbacher, P. M., Palsa, R., Streicher, O., et al. 2020, A&A, 641, A28
- Woodland, M., Mannings, A., Prochaska, J., et al. 2024, in American Astronomical Society Meeting Abstracts, Vol. 243, American Astronomical Society Meeting Abstracts, 359.07
- Yao, J. M., Manchester, R. N., & Wang, N. 2017, The Astrophysical Journal, 835, 29
- Zhang, G. Q., Yu, H., He, J. H., & Wang, F. Y. 2020, ApJ, 900, 170

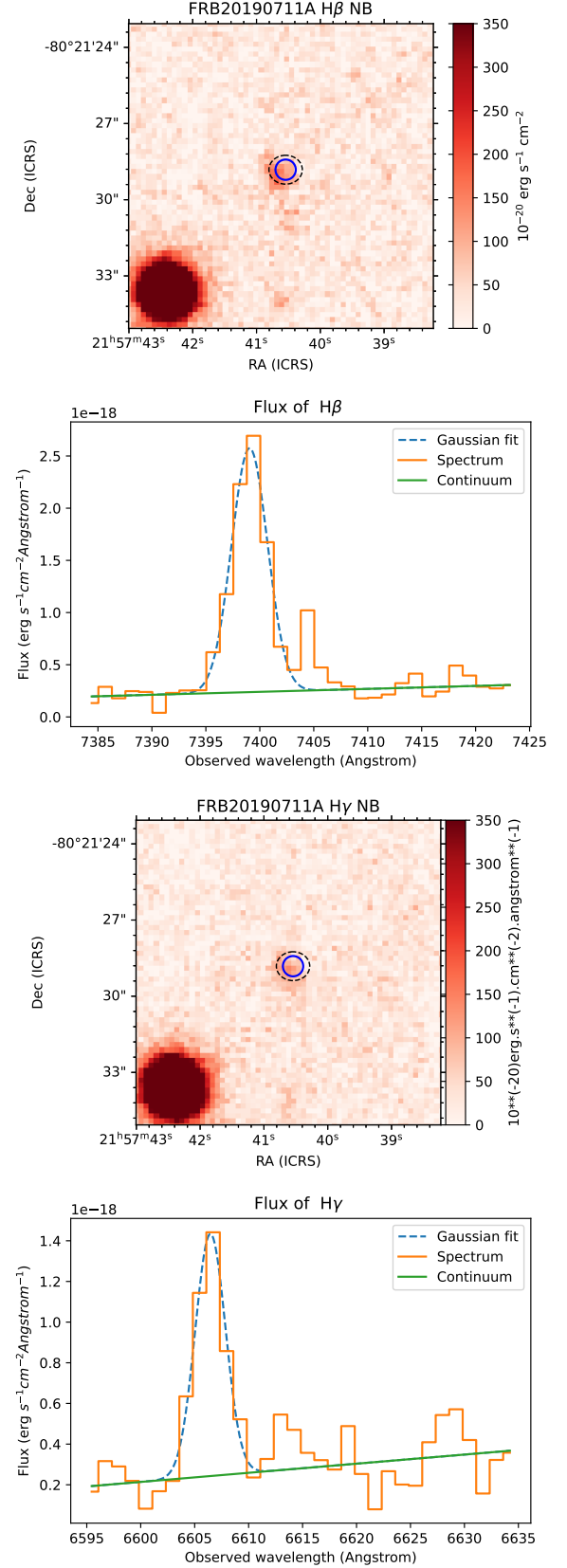


Fig. A.5. Same as Figure 1 but for FRB20190711A. In this case, instead of using $H\alpha$ we use $H\beta$ and $H\gamma$.

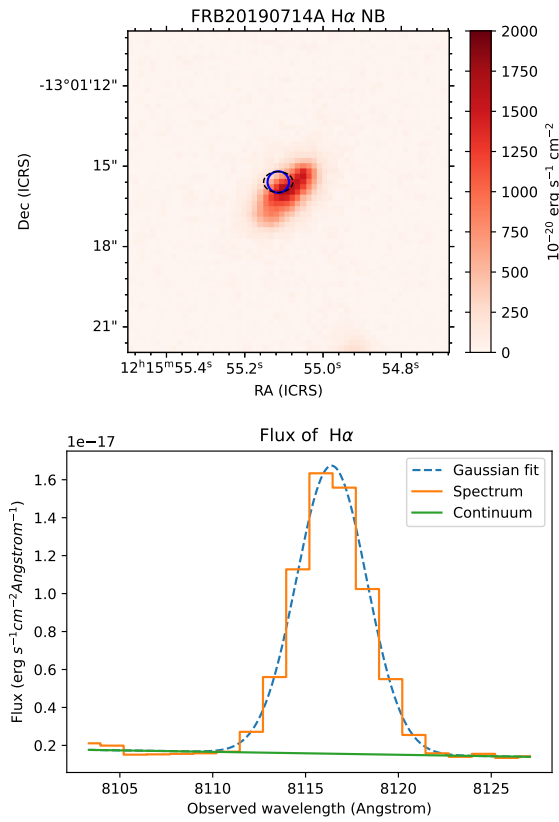


Fig. A.6. Same as Figure 1 but for FRB20190714A.

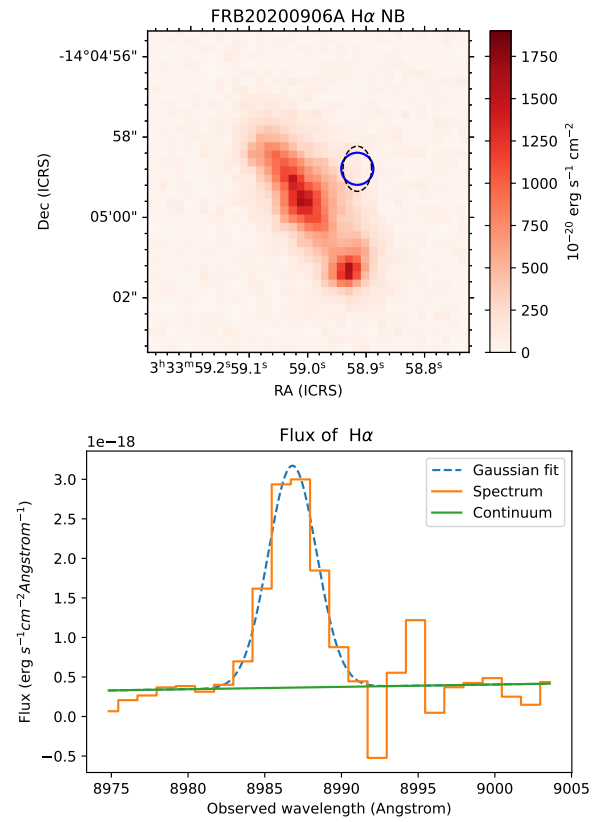


Fig. A.8. Same as Figure 1 but for FRB20200906A.

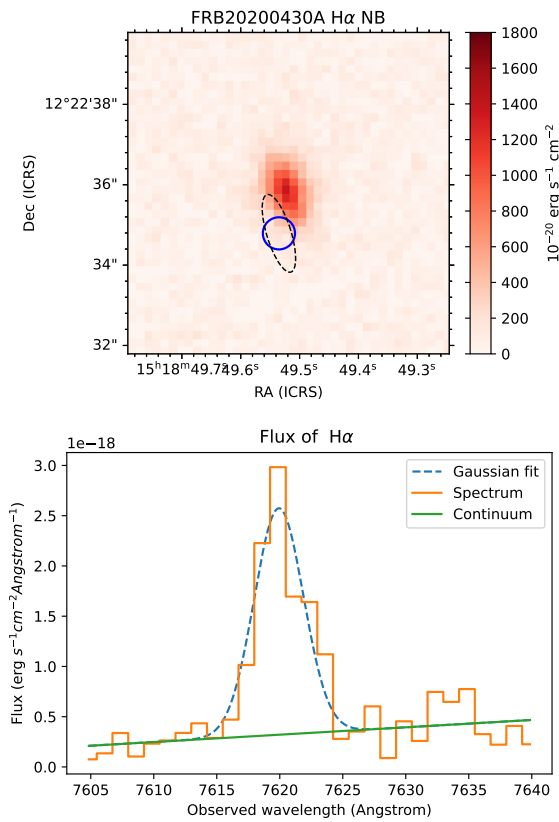


Fig. A.7. Same as Figure 1 but for FRB20200430A.

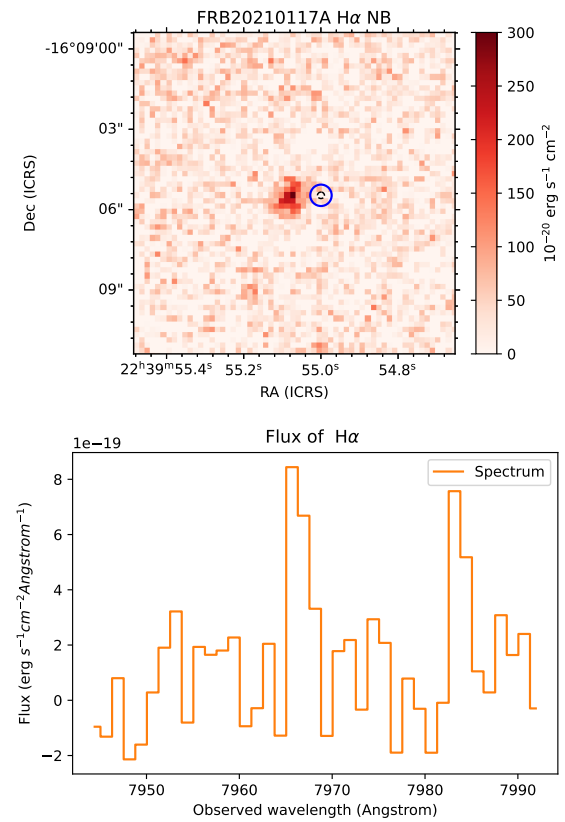


Fig. A.9. Same as Figure 1 but for FRB20210117A. In this case, we cannot fit a Gaussian and thus just report a 2σ upper limit.

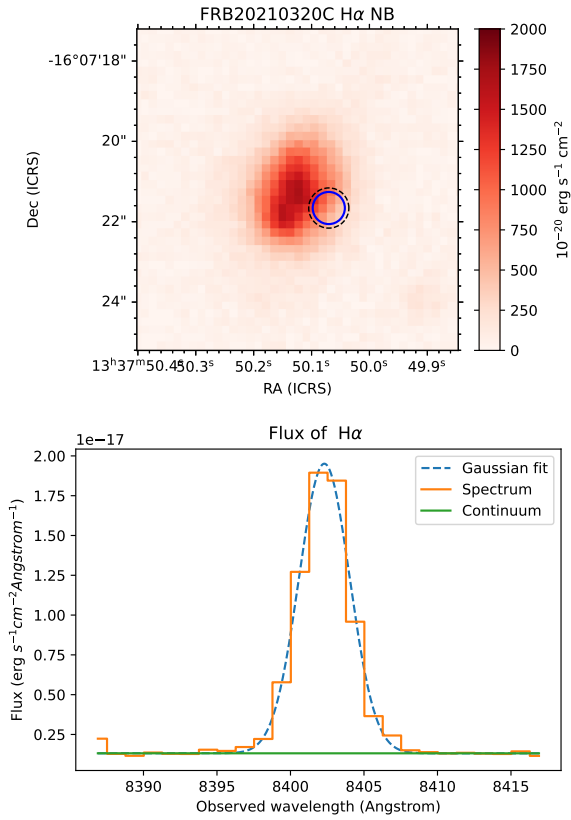


Fig. A.10. Same as Figure 1 but for FRB20210320C.

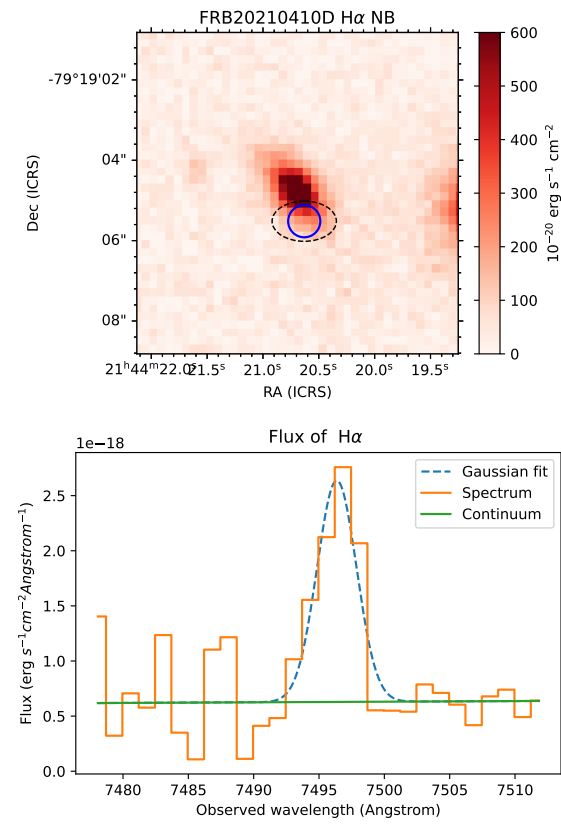


Fig. A.11. Same as Figure 1 but for FRB20210410D.

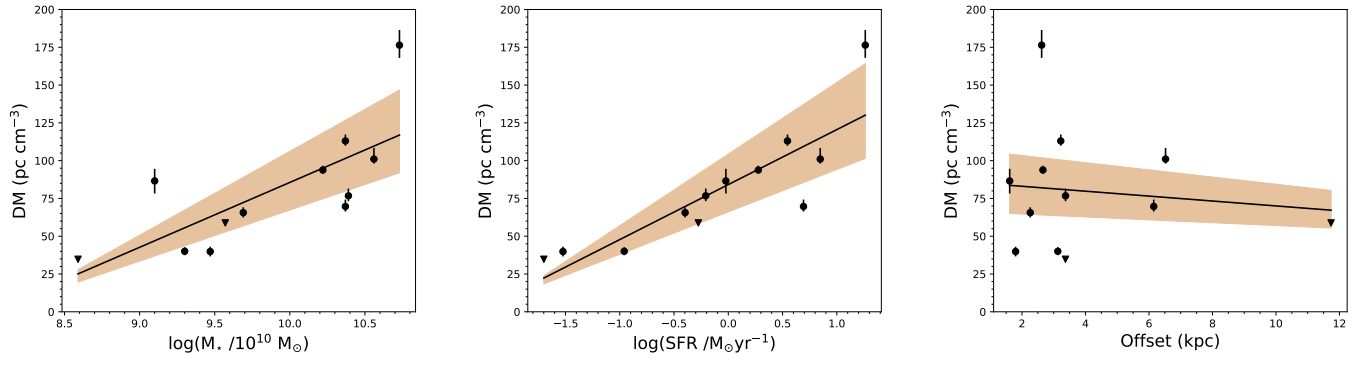


Fig. C.1. $\text{DM}_{\text{host}}^{\text{direct}}$ vs. stellar mass (in log scale; left), SFR (in log scale; middle) and projected distance (right) of the host galaxies. The black points and the black lines are the same as those in Figure 6. The shaded area corresponds to our estimated systematic uncertainty (see Section 4.5).